Elastic and thermal properties of the layered thermoelectrics BiOCuSe and LaOCuSe

S. K. Saha[1,*] and G. Dutta[2]

[1]*Department of Physics, Indian Institute of Science, Bangalore 560012, India*

[2]*Department of Physics, Balurghat College, P.O. Balurghat 733101, West Bengal, India*

(Received 8 December 2015; revised manuscript received 5 September 2016; published 30 September 2016)

We determine the elastic properties of the layered thermoelectrics BiOCuSe and LaOCuSe using first-principles density functional theory calculations. To predict their stability, we calculate six distinct elastic constants, where all of them are positive, and suggest mechanically stable tetragonal crystals. As elastic properties relate to the nature and the strength of the chemical bond, the latter is analyzed by means of real-space descriptors, such as the electron localization function (ELF) and Bader charge. From elastic constants, a set of related properties, namely, bulk modulus, shear modulus, Young's modulus, sound velocity, Debye temperature, Grüneisen parameter, and thermal conductivity, are evaluated. Both materials are found to be ductile in nature and not brittle. We find BiOCuSe to have a smaller sound velocity and, hence, within the accuracy of the used Slack's model, a smaller thermal conductivity than LaOCuSe. Our calculations also reveal that the elastic properties and the related lattice thermal transport of both materials exhibit a much larger anisotropy than their electronic band properties that are known to be moderately anisotropic because of a moderate effective-electron-mass anisotropy. Finally, we determine the lattice dynamical properties, such as phonon dispersion, atomic displacement, and mode Grüneisen parameters, in order to correlate the elastic response, chemical bonding, and lattice dynamics.

DOI: 10.1103/PhysRevB.94.125209

I. INTRODUCTION

BiOCuSe-based materials, which belong to a class of layered semiconductors, have been attracting increasing attention since they were reported as promising thermoelectric (TE) materials in 2010. This promise is mainly based on their intrinsically low thermal conductivity and tunable functionalities. In the past few years, the TE performance (ZT) of BiOCuSe has significantly been increased from 0.53 for pristine samples to 1.4 by optimization through dopants and texturation [1]. With doping of various metals, such as monovalent Na, K, and Ag [2–4], divalent Mg, Ca, Sr, Ba, Pb, and Zn [5–10], and trivalent La [11], and by introducing vacancies [12], the electrical transport properties of BiOCuSe have been improved remarkably, due to the increase in the concentration of carriers. Such doping [3–10] or/and vacancies [12,13] in BiOCuSe are also known to reduce its lattice thermal conductivity effectively by point defect scattering of phonons.

Although the electronic properties of BiOCuSe-based materials have been widely studied and the enhancement of the power factor has been well explained, surprisingly little is known about their elastic properties. Elastic properties are linked to the material's strength, specific heat, thermal expansion, phonon spectra, sound velocity, Grüneisen parameter (GP), Debye temperature, and melting point. To design thermoelectric modules suitable for long-term elevated temperature use, information about their elastic properties is extremely important, particularly to predict their stability, strength, and aging behavior and to determine their suitability for use in industry as high-performance thermoelectrics. The lack of such information has thwarted the fundamental understanding of BiOCuSe-based materials and their application in thermoelectric devices. Also, it hinders their fabrication, for instance, the stress analysis and strain energy estimation in epitaxial growth, and the simulation including elastic energy.

Motivated by these considerations, in this article, a systematic study of the elastic properties of BiOCuSe, along with a comparison to LaOCuSe, is performed using first-principles density functional theory (DFT) calculations. Elastic constants are calculated to determine the mechanical response of the materials to external stresses, as characterized by the bulk modulus (B), shear modulus (G), Young's modulus (Y), and Poisson's ratio (ν). The values of the elastic constants—which provide us with valuable information about the bonding characteristics, heat conductivity, and their anisotropic character—are needed to design and characterize new devices effectively.

II. METHODOLOGY

Our calculations are performed using the QUANTUM ESPRESSO [14–16] implementation of DFT, with the Perdew-Burke-Ernzerhof-for-solid (PBEsol) [17,18] exchange-correlation functional and projector augmented wave (PAW) potential [19–21] to represent the interaction between ionic cores and valence electrons. Kohn-Sham wave functions are represented using a plane wave basis truncated at an energy cutoff of 50 Ry and the Brillouin zone integrations are done on a uniform Monkhorst-Pack **k** grid of $11\times11\times5$. Structural relaxation is carried out so as to minimize the forces acting on each of the atoms using the Broyden-Flecher-Goldfarb-Shanno (BFGS)-based method [22].

III. RESULTS AND DISCUSSIONS

BiOCuSe and LaOCuSe (MOCuSe, M = Bi and La) adopt the ZrSiCuAs-type structure (see Fig. 1) in the tetragonal $P4/nmm$ space group (No. 129), and are isostructural to the superconducting oxypnictides LnOFePn (Ln = La, Pr, Ce, and Sm; Pn = P and As) [23]. The atomic positions are M: $2c$ $(1/4,1/4,z_M)$, O: $2a$ $(3/4,1/4,0)$, Cu: $2b$ $(3/4,1/4,1/2)$, and Se: $2c$ $(1/4,1/4,z_{Se})$, where z_M and z_{Se} are the so-called internal coordinates (see Table I). Our PBEsol estimates of the equilibrium in-plane (out-of-plane) lattice spacings are

*Corresponding author: sks.cmt@gmail.com

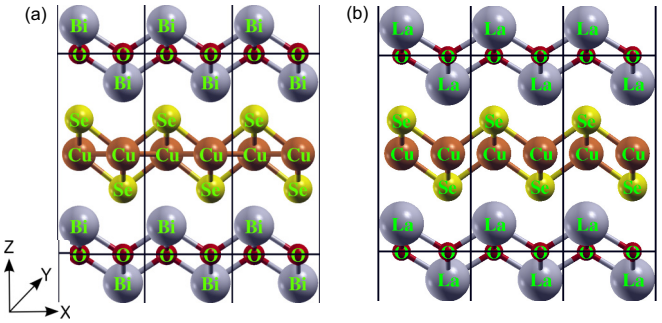

FIG. 1. Crystal structure of naturally occurring superlattice materials (a) BiOCuSe and (b) LaOCuSe, adopting the quaternary equiatomic ZrCuSiAs-type structure ($P4/nmm$ space group) with only eight atoms in the tetragonal primitive unit cell. The cell enclosed by the thin black lines represents the primitive unit cell.

$a = 3.9029$ ($c = 8.9186$) Å for BiOCuSe and $a = 4.0230$ ($c = 8.6509$) Å for LaOCuSe, in good agreement with the respective experimentally measured values of $a = 3.9213$ ($c = 8.9133$) Å for BiOCuSe and $a = 4.0670$ ($c = 8.8006$) Å for LaOCuSe. In this natural superlattice structure, the antifluoritelike $(Cu_2Se_2)^{2-}$ chalcogenide layers of slightly distorted edge-sharing $CuSe_4$ tetrahedra alternate with fluoritelike $(M_2O_2)^{2+}$ oxide layers, stacked along the c axis of the tetragonal cell. For both materials, the insulating $(M_2O_2)^{2+}$ oxide layers with ionic bonds act as charge reservoirs, and the conductive $(Cu_2Se_2)^{2-}$ selenide layers with covalent bonds constitute the conduction pathway for carrier transport, which can be controlled to achieve high electrical conductivity [27].

The bond lengths provide information about the physical nature of the chemical bonds [28]. It is expected that the calculated bond length (d) of an ionic bond is close to the sum $d_s = r_c + r_a$, where the ionic radius of a cation is r_c and that of a neighboring anion is r_a [29]. The Cu-Se bonds

TABLE I. Calculated crystal parameters of BiOCuSe and LaOCuSe as compared to experimental values.

		BiOCuSe		LaOCuSe	
		PBEsol	Experiment	PBEsol	Experiment
a (Å)		3.9029	3.9213[a]	4.0230	4.0670[c]
c (Å)		8.9186	8.9133[a]	8.6509	8.8006[c]
z_{Se}		0.6736	0.6802[a]	0.6696	0.6698[c]
z_M		0.1420	0.1411[a]	0.1423	0.1396[c]
Bond length (Å)					
M-O		2.3266	2.326[a]	2.3584	2.377[c]
M-Se		3.2123	3.208[a]	3.2770	3.328[c]
M-Cu		3.7417		3.6907	
Cu-Se		2.4912	2.526[a]	2.4901	2.523[c]
Bond angle (deg)					
M-O-M	(×4)	107.25	106.9[b]	105.81	105.53[c]
	(×2)	114.02	114.6[b]	117.06	117.67[c]
Se-Cu-Se	(×4)	112.73	113.6[b]	110.33	110.52[c]
	(×2)	103.13	101.4[b]	107.77	107.40[c]

[a]Reference [24].
[b]Reference [25].
[c]Reference [26].

in both systems are reasonably explained by the ionic radii picture because the calculated bond lengths (see Table I) are very close to the d_s value (2.58 Å). In contrast, the Bi-O and La-O bonds ($d = 2.33$ Å, $d_s = 2.57$ Å, and $d = 2.36$ Å, $d_s = 2.56$ Å, respectively) have less ionic character than the Cu-Se bonds, indicating that both Bi-O and La-O bonds are stiffer than the Cu-Se bond. Table I further shows that the Bi-O and Bi-Se bond lengths in BiOCuSe are shorter than the La-O and La-Se bond lengths in LaOCuSe, respectively. In contrast, the Bi-Cu distance in BiOCuSe is longer than the La-Cu distance in LaOCuSe, indicating a weaker Cu bond in the former than in the latter. In addition, the lengths of the La-Se and La-Cu bonds in LaOCuSe (3.33 and 3.69 Å) are much longer than their respective d_s values (3.14 and 2.07 Å). Likewise, the lengths of the Bi-Se and Bi-Cu bonds in BiOCuSe (3.21 and 3.74 Å) are much longer than their respective d_s values (3.15 and 2.08 Å). The difference between d and d_s for the Bi-Se bond in BiOCuSe is smaller than that for the La-Se bond in LaOCuSe. In contrast, the difference between d and d_s for the Bi-Cu bond in BiOCuSe is larger than that for the La-Cu bond in LaOCuSe. Although the Cu-Se bond length is almost equal in BiOCuSe and LaOCuSe, $CuSe_4$ distortion is larger in BiOCuSe than in LaOCuSe. The larger distortion indicates a softer lattice and higher anharmonicity, which should dissipate phonons more easily in the former than in the latter. The Se-Cu-Se bond angle is closer to that in a regular tetrahedron (109.5°). On the other hand, the O-Bi-O angle in BiOCuSe is much smaller than the O-La-O angle in LaOCuSe.

Figure 2 shows the pattern of the calculated valence charge density distribution of BiOCuSe and LaOCuSe with a cut by the [100] plane. The electronic charge distributions at the Bi atoms agglomerate more away from the Bi-O bonds, as compared to that around the La atoms. These electrons are not regarded as lone pairs in a strict sense (of chemical inertness). However, this result is consistent with a revised lone pair model [30], whereby the chemical interaction between the Bi 6s and O 2p results in the formation of electron lone pairs, combined with a structural distribution allowing mixing between the Bi 6s-O 2p and Bi 6p states.

For both materials, we also calculate (see Fig. 3) the electron localization function (ELF) [31], which has often been used to characterize the degree of electron localization and to quantitatively identify the character of the chemical bond between atoms. ELF is defined as $\mathrm{ELF}(\mathbf{r}) = \frac{1}{1+[D(\mathbf{r})/D_h(\mathbf{r})]^2}$, where $D(\mathbf{r})$ and $D_h(\mathbf{r})$ represent the Pauli kinetic energy densities, respectively, for the actual system and a homogeneous electron gas with the same density as the actual system at a given point of real space $\mathbf{r}$. ELF = 0 corresponds to no localization (regions without any electron), ELF = 0.5 reflects the behavior of a homogeneous electron distribution (as found in regions where the bonding has a metallic character), and ELF = 1 indicates full localization (as found in regions of core shells, covalent bonds, and lone pairs). Figure 3 plots the ELF of the $P4/nmm$ structure of both materials, depicting that the charges are located around the Bi (La), O, and Se atoms in BiOCuSe (LaOCuSe). Bader charge analysis [32] further shows that in BiOCuSe (in LaOCuSe), each Bi (La) atom transfers 1.16e (1.28e) to the O atoms and 0.5e (0.6e) to the Se atoms. Both ELF and Bader

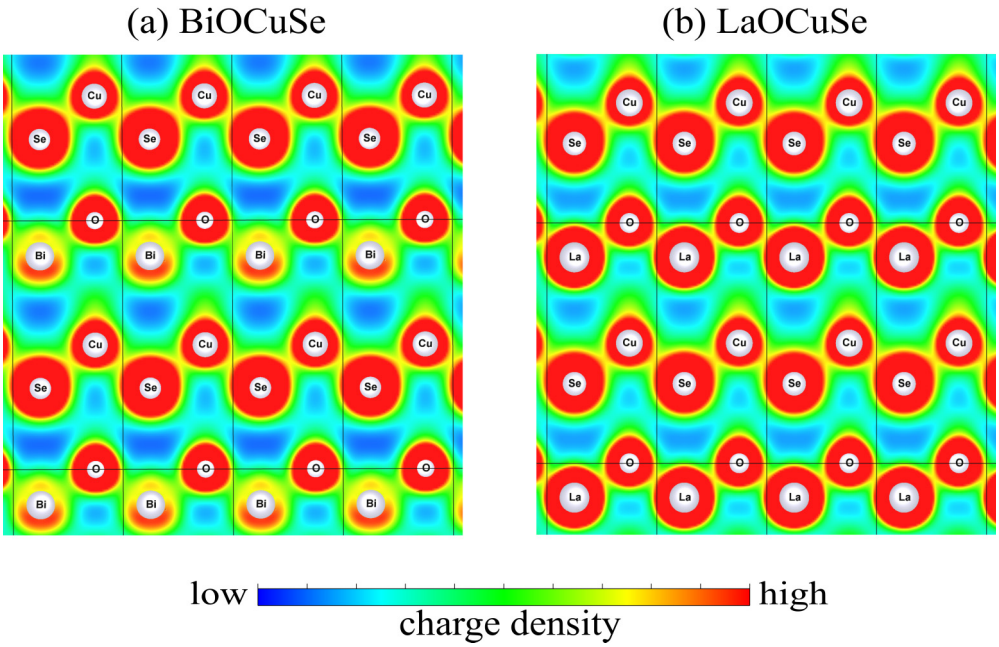

FIG. 2. The pattern of the calculated valence charge density distribution with a cut by the [100] plane for (a) BiOCuSe and (b) LaOCuSe. Blue (deep dark) represents low valence charge while red (light dark) represents a high concentration of valence charge.

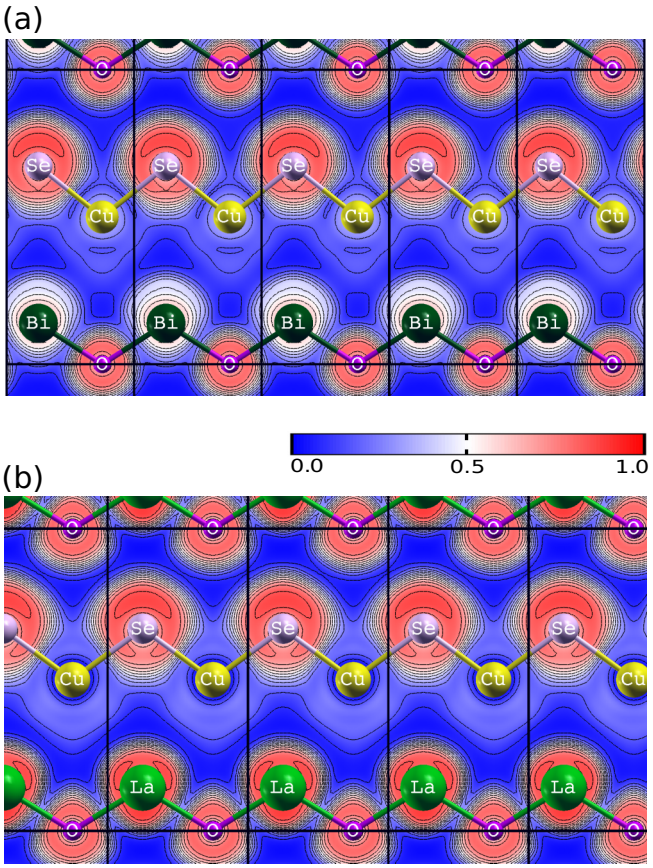

FIG. 3. The map of the calculated electron localization function with a cut by the [100] plane for (a) BiOCuSe and (b) LaOCuSe. Blue (ELF = 0.0, deep dark) represents no electron localization, red (ELF = 1.0, light dark) represents full electron localization, while white (ELF = 0.5, bright) corresponds to the behavior of a homogeneous electron distribution.

analysis suggest a weak bonding of copper atoms within the structure of BiOCuSe and of LaOCuSe. The weak bonding of copper atoms is consistent with the fact that the Cu-Se distances in BiOCuSe and LaOCuSe are longer than those reported for other compounds containing Cu^{+} in a tetrahedral coordination, for example, the Cu-Se distance in $CuGaSe_2$ is 2.385 Å [33], significantly shorter than the values of 2.526 and 2.523 Å found for BiOCuSe and LaOCuSe, respectively. Our calculations of the deformation energy also demonstrate that Cu-Se bonds are much weaker than both Bi-O and La-O bonds. We find that the total energy is minimally affected by a Cu-Se bond compression of up to 12% of its equilibrium bond length.

Figure 4 shows the electronic band structures of BiOCuSe and LaOCuSe. Both are multiband semiconductors. Both materials are known to form p-type semiconductors and, hence, the top part of the valence band has the greatest effect on its electrical properties. For LaOCuSe, the valence-band maximum (VBM) and conduction-band minimum (CBM) both are found to locate on the Γ point and, hence, LaOCuSe is a direct-band gap semiconductor. For BiOCuSe, the VBM and CBM are found to locate on the M-Γ line and at the Z points, respectively. As a result, BiOCuSe is an indirect-band gap semiconductor. The calculated dispersion along the Γ-X-M line is greater than that along the Γ-Z-R line. This leads to a mixture of light and heavy bands in the upper valence band of BiOCuSe, with effective masses of $0.16m_e$ (where m_e denotes the true mass of an electron) and $1.02m_e$, respectively. The above mixture of bands gives an average effective mass of $0.59m_e$, close to the previous estimation of $0.6m_e$ [9]. The mixture of light and heavy bands is beneficial for thermoelectric performance [34], as the light bands are favorable for the carrier mobility, and thus the electrical conductivity, whereas the heavy bands lead to a steeper density of states close to the Fermi level and thus to a higher Seebeck

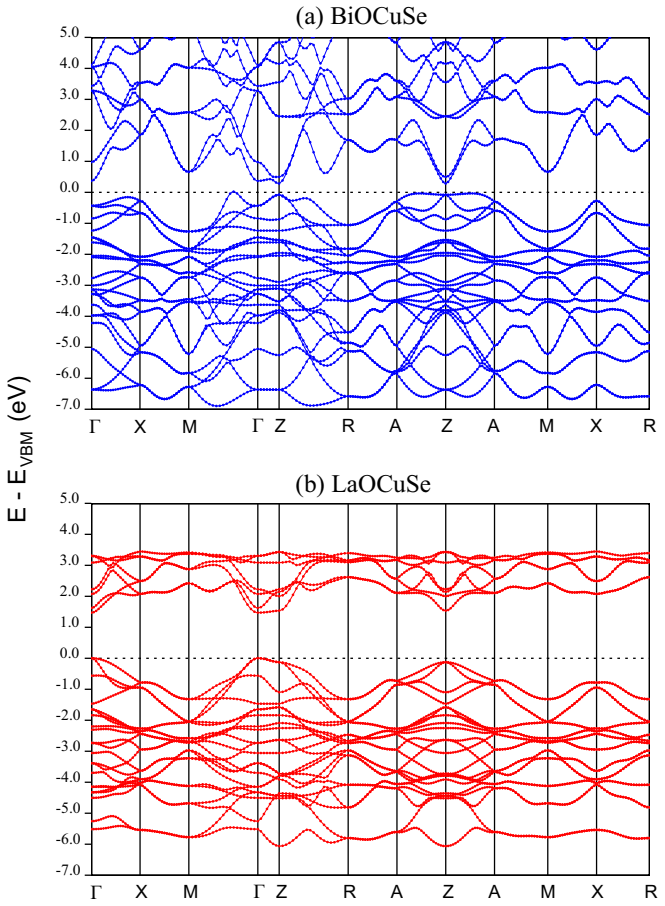

FIG. 4. Electronic energy band structure of (a) BiOCuSe and (b) LaOCuSe. The dashed lines represent the valence-band maximum (VBM) levels and are set to zero.

coefficient. A layered crystal structure is expected to show a strong anisotropy of the electronic behavior, with a large electrical conductivity within the conducting layer in the a,b plane and a low electrical conductivity perpendicular to the conducting layer along the c axis. However, the electronic band structure is not as anisotropic as could have been expected: Although the band dispersion is larger along the Γ-X-M line than along the Γ-Z one, the out-of-plane effective mass remains moderate (about 14% heavier than the in-plane effective mass), suggesting a somewhat three-dimensional (3D) character of the electrical transport properties. Indeed, the in-plane and cross-plane Seebeck coefficients of highly textured BiOCuSe samples are almost the same [1]. This observation can be explained by a moderate Bi-Se orbital overlap. While the electrical behaviors of both materials are found to be moderately anisotropic because of the moderate effective mass anisotropy, it is now of immediate interest to see whether or not their elastic and related lattice thermal transport properties exhibit a much larger anisotropy.

Since BiOCuSe and LaOCuSe crystallize in tetragonal symmetry, only six elastic constants are required to describe their mechanical response. The values of these constants (C_{ij}, viz., C_{11}, C_{12}, C_{13}, C_{33}, C_{44}, and C_{66}, and, equivalently, $S_{ij} = \frac{1}{C_{ij}}$) for MOCuSe are estimated by calculating the stress tensors on applying different deformations to the equilibrium tetragonal lattice (see Table II). C_{11} and C_{33} reflect the stiffness to uniaxial strains along the crystallographic a and c axes, respectively, while the elastic constants C_{12}, C_{13}, C_{44}, and C_{66} are related to the elasticity in shape. Table II shows that the values of C_{11} are much higher than C_{33}, suggesting that both materials are stiffer for strains along the a axis than along the c axis. All these elastic constants are positive and satisfy the well-known Born criteria for mechanically stable tetragonal crystals: $C_{11} > 0$, $C_{33} > 0$, $C_{44} > 0$, $C_{66} > 0$, $(C_{11} - C_{12}) > 0$, $(C_{11} + C_{33} - 2C_{13}) > 0$, and $2(C_{11} + C_{12}) + C_{33} + 4C_{13} > 0$. It is also worth mentioning that we find LaOCuSe to have larger C_{11} (smaller C_{12}) than BiOCuSe, leading to a larger positive shear constant $C' = \frac{C_{11}-C_{12}}{2}$ for LaOCuSe (64 GPa) than for BiOCuSe (42 GPa). A bigger positive value for this shear constant implies a larger mechanical stability of LaOCuSe at the simulation temperature of 0 K. A smaller C_{11} in BiOCuSe than in LaOCuSe is in conformity with the weaker Cu bond in the former than in the latter, as found above. In addition, the larger value of C_{12} in BiOCuSe than in LaOCuSe implies that the atomic configurations and bonding in the directions [100] and [010] are more strongly interrelated in the former than in the latter. This appears to be in conformity with our above finding that $CuSe_4$ distortion is larger in BiOCuSe than in LaOCuSe, even though the Cu-Se bond length is almost equal in both. This larger distortion as well as the weaker Cu bond in BiOCuSe than in LaOCuSe indicate a softer lattice and higher anharmonicity which can dissipate phonons more easily in the former than in the latter.

From the calculated elastic constants, the macroscopic mechanical parameters, viz., bulk modulus (B) and shear

TABLE II. Calculated single-crystal relaxed-ion elastic constants C_{ij} (in GPa); compliances S_{ij} (in Mbar^{-1}); bulk moduli B_X (in GPa^{-1}, $X = V$, R, and H standing for Voigt, Reuss, and Voigt-Reuss-Hill approximations, respectively); shear moduli G_X (in GPa^{-1}); B_X/G_X ratios; compressibilities β_X (in GPa^{-1}); Young's moduli Y_X (in GPa); and Poisson ratios ν_X of BiOCuSe and LaOCuSe in their $P4/nmm$ phase. All quantities are calculated at the respective theoretical equilibrium volume obtained with the PBEsol functional.

	BiOCuSe	LaOCuSe		BiOCuSe	LaOCuSe		BiOCuSe	LaOCuSe		BiOCuSe	LaOCuSe		BiOCuSe	LaOCuSe
C_{11}	153.3	176.3	S_{11}	0.955	0.720	B_V	89.32	88.08	B_R	84.80	83.10	B_H	87.06	85.56
C_{12}	69.2	49.1	S_{12}	−0.235	−0.067	G_V	35.49	39.24	G_R	33.84	34.90	G_H	34.67	37.07
C_{13}	64.7	60.3	S_{13}	−0.466	−0.391	$\frac{B_V}{G_V}$	2.18	1.99	$\frac{B_R}{G_R}$	2.21	2.02	$\frac{B_H}{G_H}$	2.19	2.00
C_{33}	100.1	100.6	S_{33}	1.603	1.463	β_V	0.010693	0.010868	β_R	0.011104	0.011455	β_H	0.010894	0.011154
C_{44}	31.7	28.0	S_{44}	3.145	3.568	Y_V	94.02	102.51	Y_R	89.60	91.84	Y_H	91.81	97.17
C_{66}	44.6	45.7	S_{66}	2.244	2.190	ν_V	0.325	0.306	ν_R	0.324	0.316	ν_H	0.324	0.311

modulus (G), are calculated using the Voigt (V) [35], Reuss (R) [36], and Voigt-Reuss-Hill (H) approaches [37] in the following forms:

$$B_V = \frac{1}{9}\{2(C_{11}+C_{12})+C_{33}+4C_{13}\},$$

$$G_V = \frac{1}{30}\{M+3C_{11}-3C_{12}+12C_{44}+6C_{66}\},$$

$$B_R = \frac{C^2}{M},$$

$$G_R = 15\left\{\frac{18B_V}{C^2}+\frac{6}{C_{11}-C_{12}}+\frac{6}{C_{44}}+\frac{3}{C_{66}}\right\}^{-1},$$

where $C^2=(C_{11}+C_{12})C_{33}-2C_{13}^2$ and $M=C_{11}+C_{12}+2C_{33}-4C_{13}$. The results obtained are summarized in Table II. It is known that the Voigt (V) bound is obtained by the average polycrystalline moduli based on an assumption of uniform strain throughout a polycrystal and is the upper limit of the actual effective moduli, while the Reuss (R) bound is obtained by assuming a uniform stress and is the lower limit of the actual effective moduli [37]. According to Hill, the Voigt and Reuss averages are limits and the actual effective modules for polycrystals could be approximated by the arithmetic mean of these two bounds. According to the Pugh criterion [38], a material is ductile if the B/G ratio is greater than 1.75. Hence, both the materials in this study are ductile and not brittle.

The percentage anisotropy in compressibility and shear are defined as $A_C=\frac{B_V-B_R}{B_V+B_R}$ and $A_S=\frac{G_V-G_R}{G_V+G_R}$, respectively. A value of zero corresponds to elastic isotropy and a value of 100% is the largest possible anisotropy. Within the PBEsol approximation herein, BiOCuSe possesses $A_C\sim 2.6\%$ and $A_S\sim 2.4\%$, while LaOCuSe acquires $A_C\sim 2.9\%$ and $A_S\sim 5.9\%$, indicating that LaOCuSe is relatively more elastically anisotropic in nature. Also, the ratio of bulk modulus along the a axis to that along the c axis can be calculated by [39] $\frac{B_a}{B_c}=\frac{(c_{11}-c_{13})+(c_{12}-c_{13})}{c_{33}-c_{13}}$. The obtained $\frac{B_a}{B_c}=2.640$ (2.607) for BiOCuSe (for LaOCuSe), showing strong anisotropy in the bulk modulus for both materials.

Furthermore, from B and G, Young's modulus (Y) and the Poisson ratio (ν) are evaluated as $Y=\frac{9BG}{3B+G}$ and $\nu=\frac{3B-2G}{6B+2G}$, respectively. All these parameters are listed in Table II. In the mechanics of deformable bodies, the tendency for a material to expand or shrink in a direction perpendicular to a loading direction is known as the Poisson effect [40]. It is a well-known fact today that its theoretical value for an isotropic material cannot be less than -1.0 nor greater than 0.5 due to the fact that Young's, shear, and bulk moduli must be positive, based on thermodynamic restrictions. The typical value of the Poisson ratio is about 0.2 for covalent materials such as silicon, whereas it is about 0.3–0.4 for ionic materials and 0.5 for a pure-ionic limit.

The propagation velocities of longitudinal (v_l) and transverse (v_t) acoustic waves are derived from

$$v_l=\sqrt{\frac{Y(1-\nu)}{\rho(1+\nu)(1-2\nu)}}=\sqrt{\frac{B+4G/3}{\rho}}$$

and

$$v_t=\sqrt{\frac{Y}{2\rho(1+\nu)}}=\sqrt{\frac{G}{\rho}},$$

TABLE III. Calculated longitudinal (v_l), transverse (v_t), and average (v_m) sound velocities (in m/s), Debye temperature (Θ_D, in K), and Grüneisen parameter (γ) for BiOCuSe and LaOCuSe in their $P4/nmm$ phase.

	v_l	v_t	v_m	Θ_D	γ
BiOCuSe	3855.3	1966.2	2187.4	253.2	1.93
LaOCuSe	4375.1	2292.5	2519.3	288.9	1.84

where ρ is the mass density and the others are as defined previously. The Debye temperature (Θ_D) [41] is calculated from the relation $\Theta_D=\frac{h}{k_B}\left(\frac{3n}{4\pi\Omega}\right)^{1/3}v_a$, where h and k_B are Planck and Boltzmann constants, respectively, n is the number of atoms in the cell, Ω is the cell volume, and v_a is the average sound wave velocity. The v_m is given in terms of v_l and v_t as

$$v_m=\left[\frac{1}{3}\left(\frac{1}{v_l^3}+\frac{2}{v_t^3}\right)\right]^{-1/3}.$$

The v_m, obtained using theoretical v_l and v_t provided in Table III, is in reasonable agreement with the experimentally measured value of 2112 m/s for BiOCuSe [42]. The difference between theory and experiment can be attributed to the difference in lattice parameters arising from thermal effects, or/and to the uncertainty in the ultrasonic pulse echo measurement. The v_l and v_t are essentially harmonic parameters while their ratio v_l/v_t is an anharmonic quantity which depends on the ratio between the axial and shear rigidities of interatomic bonds and thus is related to the Grüneisen parameter γ, which suggests the degree of anharmonicity. The γ values are calculated from [43] $\gamma=\frac{9-12(\frac{v_t}{v_l})^2}{2+4(\frac{v_t}{v_l})^2}$. A larger γ indicates higher anharmonicities of the chemical bond which generally drives greater phonon-phonon scatterings (umklapp or/and normal) and thus shorter relaxation times [44,45]. Assuming the heat is conducted only by acoustic phonons via these umklapp scattering processes, the thermal conductivity can be evaluated by Slack's equation [46] $\kappa=3.1\times10^{-6}\frac{\bar{M}\Theta^3\delta}{\gamma^2 n^{2/3}T}$ in W m^{-1} K^{-1}, where $\bar{M}$ is the average atomic mass in amu, Θ is the Debye temperature in K, δ^3 is the volume per atom in Å^3, n is the number of atoms in the primitive unit cell, and γ is the average Grüneisen parameter. This relation gives $\kappa=0.86$ W m^{-1} K^{-1} at $T=923$ K for BiOCuSe with $\gamma_\alpha=1.93$ and $\Theta=253.2$ K (see Table III), whereas $\kappa=1.46$ W m^{-1} K^{-1} at $T=923$ K for LaOCuSe with $\gamma_\alpha=1.84$ and $\Theta=288.9$ K (see Table III). This PBEsol estimate of the κ of BiOCuSe is about 1.7 times lower than that of its isostructural analog LaOCuSe. Our estimated value is very different from the experimental observation as the measured κ of BiOCuSe ($\sim$0.45 W m^{-1} K^{-1} at 923 K [9]) is about four times lower than that of LaOCuSe (2.1 W m^{-1} K^{-1} at room temperature [47]). This discrepancy suggests that the effect of optical-acoustic phonon scattering should not be ignored. The optical-acoustic phonon scattering is expected to be much stronger in BiOCuSe than in LaOCuSe because the former is heavier (Bi atoms being heavier than La atoms) and is expected to have softer [48,49] and more anharmonic optical phonons than the latter.

TABLE IV. The anisotropic sound velocities (in m/s) of tetragonal BiOCuSe and LaOCuSe.

	[100]			[001]		
Direction	$[100]v_l$	$[001]v_{t_1}$	$[010]v_{t_2}$	$[001]v_l$	$[100]v_{t_1}$	$[010]v_{t_2}$
BiOCuSe	4139	1888	2231	3344	1888	1888
LaOCuSe	4999	1993	2545	3777	1993	1993

In order to understand the anisotropy of the thermal conductivity, Anatychuk and Mikhalchenko [50] used a modified version of the Slack's equation [46], $\kappa_{ii} = 3.1\times10^{-6}\frac{\bar{M}\Theta_{ii}^3\delta}{\gamma_{ii}^2 n^{2/3}T}$ in W m^{-1} K^{-1}, where i is the crystallographic direction and where the Debye temperature Θ and Grüneisen parameter γ are replaced respectively by the Debye temperatures Θ_{ii} and the Grüneisen parameters γ_{ii}. This can indeed be defined for each i direction for an anisotropic system from the sound velocity v_i.

According to the Christoffel equation, the dependence of sound velocity on the propagating direction can be expressed as

$$v_l = \sqrt{\frac{C_{11}}{\rho}}, \quad [001]v_{t_1} = \sqrt{\frac{C_{44}}{\rho}}, \quad [010]v_{t_2} = \sqrt{\frac{C_{66}}{\rho}}$$

and

$$v_l = \sqrt{\frac{C_{33}}{\rho}}, \quad [100]v_{t_1} = [010]v_{t_2} = \sqrt{\frac{C_{44}}{\rho}},$$

where ρ is the mass density. The anisotropies in sound velocities are presented in Table IV.

In solids, the velocity of elastic wave $v \sim \sqrt{Y}$ and the lattice thermal conductivity $\kappa \sim v^3$. Hence, $\kappa \sim Y^{\frac{3}{2}}$. To give a quantitative estimation for the ratio of in-plane to out-of-plane κ, we calculate the Young's modulus Y along the a and c axes. For a transversely isotropic material with tetragonal symmetry, its physical properties are symmetric about an axis (c axis) that is normal to a plane of isotropy. For such a polar anisotropic material, the out-of-plane (c axis) and in-plane (a,b plane) Young's moduli are given by [51]

$$Y_c = C_{33} - \frac{2C_{13}C_{13}}{C_{11}+C_{12}}$$

and

$$Y_a = Y_b = \frac{(C_{11}-C_{12})(C_{11}C_{33}+C_{12}C_{33}-2C_{13}C_{13})}{C_{11}C_{33}-C_{13}C_{13}}.$$

These give $Y_c = 67.5$ GPa (68.3 GPa) and $Y_a = 116.8$ GPa (138.9 GPa) for BiOCuSe (for LaOCuSe). Both materials exhibit a much lower perpendicular Young's modulus, attesting that both possess a much lower strength of chemical bonding along the c axis and thus a lower sound velocity (Debye temperature) along that axis. Indeed, in our calculations, the Debye temperature along the c direction for BiOCuSe (for LaOCuSe) is smaller by about 1.3% (1.4%) than that along the a or b direction. This suggests that the out-of-plane thermal conductivity (κ_{cc}) in both materials is about two times smaller than the in-plane one (κ_{aa}). The effect of anisotropic anharmonicity is expected to further modify this anisotropy of heat flow.

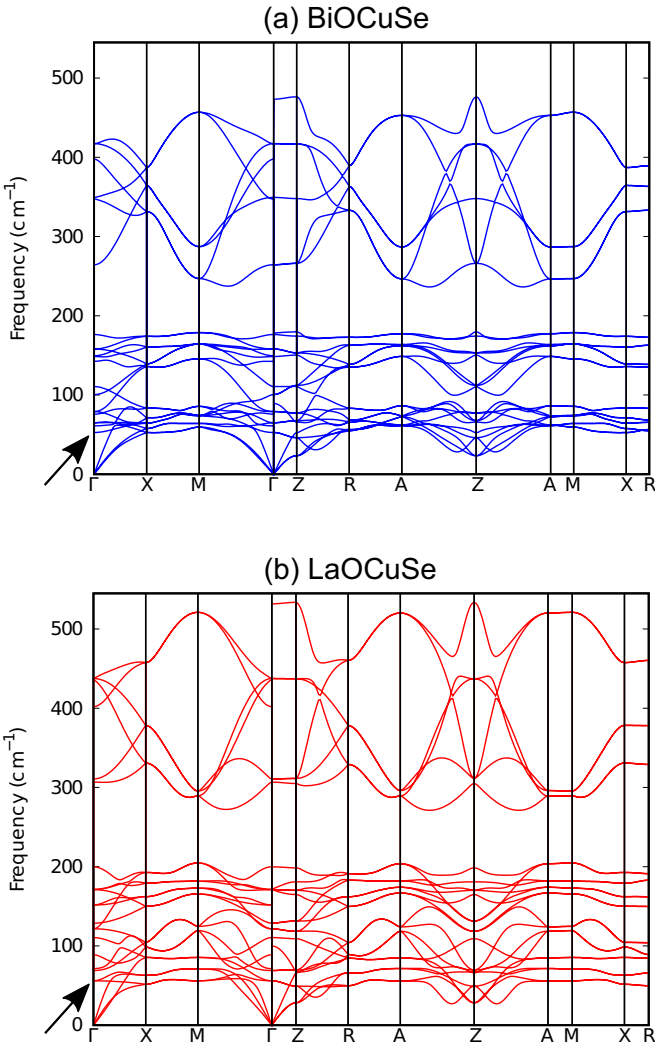

FIG. 5. Calculated phonon dispersion of (a) BiOCuSe and (b) LaOCuSe along the high-symmetry lines of the Brillouin zone. The arrow indicates the zone-center frequency of the lowest optical phonon in each material.

Finally, in order to understand the underlying mechanisms that suppress thermal conduction in BiOCuSe more than in LaOCuSe, we study the phonon dispersion (see Fig. 5) and the mode Grüneisen parameters for both materials. BiOCuSe shows the presence of a very-low-frequency manifold of optic modes centered at 53 cm^{-1} near the zone center. From the analysis of eigendisplacements of this lowest-frequency optical (LFO) mode, we find that the Cu atom (in the x or y direction) vibrates more about its equilibrium position than other atoms, physically implying the weak restoring forces on the vibrating atoms due to the existence of weak Cu bonding. Despite being very heavy, Bi atoms in the LFO mode exhibit a significantly large displacement which is, however, three times smaller than that of Cu atoms. The contribution of Cu atoms to the phonon density of states of this mode outweighs that of the heavier Bi atom, as it is three times larger than that of the latter. In LaOCuSe, the low-frequency region (centered at 62 cm^{-1}

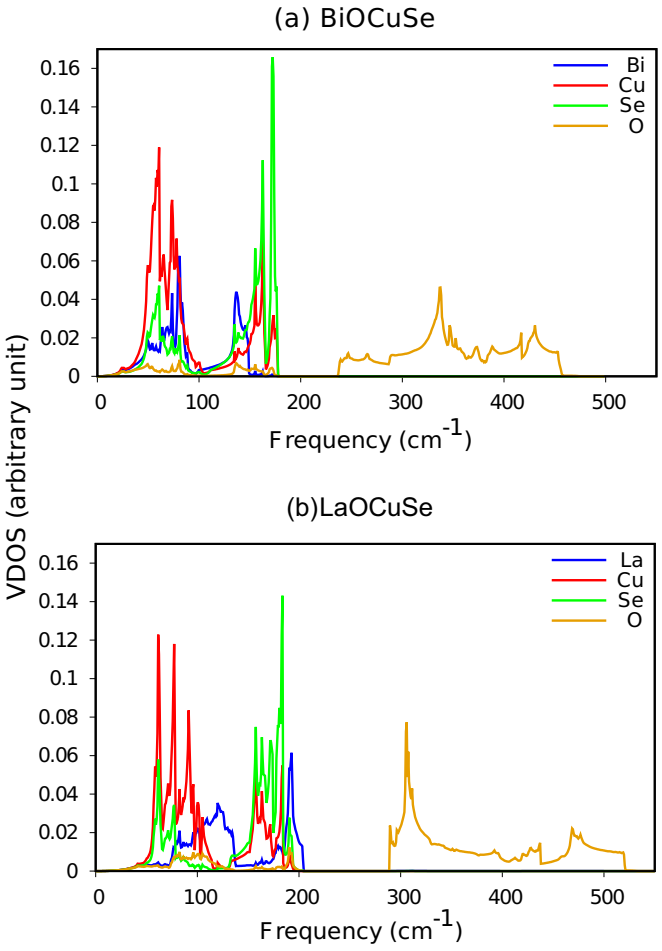

FIG. 6. Calculated vibrational density of states (VDOS) projected onto each element of (a) BiOCuSe and (b) LaOCuSe.

near the zone center) is still dominated by Cu modes as in BiOCuSe, and the La dominated vibrational modes are shifted to higher frequencies and, hence, overlap less with the Cu dominated modes as compared to BiOCuSe (see Fig. 6). This indicates that the change in the atomic mass is the main reason for the change in lattice thermal conductivity associated with Bi/La substitution. In addition, the lowest-frequency optical mode (indicated by the arrow in Fig. 5) in BiOCuSe has a larger mode GP (4.96) than that in LaOCuSe (3.89), leading to a stronger anharmonic scattering at elevated temperatures. A proper selection of atomic species, for example, a best possible rattler or/and a very heavy element, is crucial to increase the chemical bond hierarchy, elastic compliance, and phonon softness for lowering lattice thermal conductivity. A measure of the above overlap of atomic contributions (i.e., cophonicity) is a guide to properly selecting atomic species to tune specific vibrational frequencies of a given compound, particularly to engineer a low-frequency range of vibrational modes in order to design a thermoelectric material with an improved thermal resistivity.

IV. CONCLUSIONS

In conclusion, we have systematically studied the elastic properties of BiOCuSe and LaOCuSe, using first-principles DFT calculations. We have evaluated six independent elastic constants, where all of them are positive, and suggest mechanically stable tetragonal crystals. The relationship between the elastic response and chemical bonding is analyzed by means of real-space descriptors, such as the electron localization function (ELF) and Bader charge, and the relationship between the elastic and thermal properties is quantified by using the Grüneisen parameter. We have found a lower sound velocity and, hence, within the accuracy of the used Slack's model, a lower thermal conductivity in BiOCuSe than in LaOCuSe. Our calculations have also revealed that the elastic and related lattice thermal properties of both materials exhibit a much larger anisotropy than their electronic band properties. Finally, the lattice dynamical properties such as phonon dispersion, atomic displacement, and mode Grüneisen parameter are calculated in order to correlate the elastic response, chemical bonding, and lattice dynamics. The results obtained in this work should be useful for predicting the strain effect on phase transitions and designing BiOCuSe and related materials for thermoelectric applications towards alternate sources of energy that are abundant, renewable, cost effective, and environmentally friendly.

[1] J. Sui *et al.*, Energy Environ. Sci. **6**, 2916 (2013).
[2] D. Sun Lee, T.-H. An, M. Jeong, H.-S. Choi, Y. Soo Lim, W.-S. Seo, C.-H. Park, C. Park, and H.-H. Park, Appl. Phys. Lett. **103**, 232110 (2013).
[3] J. Li, J. Sui, Y. Pei, X. Meng, D. Berardan, N. Dragoe, W. Cai, and L.-D. Zhao, J. Mater. Chem. A **2**, 4903 (2014).
[4] S. G. Tan, H. Lei, D. F. Shao, H. Y. Lv, W. J. Lu, Y. N. Huang, Y. Liu, B. Yuan, L. Zu, X. C. Kan *et al.*, Appl. Phys. Lett. **105**, 082109 (2014).
[5] C. Barreteau, D. Bérardan, E. Amzallag, L. Zhao, and N. Dragoe, Chem. Mater. **24**, 3168 (2012).
[6] J. Li, J. Sui, Y. Pei, C. Barreteau, D. Berardan, N. Dragoe, W. Cai, J. He, and L.-D. Zhao, Energy Environ. Sci. **5**, 8543 (2012).
[7] J.-L. Lan, Y.-C. Liu, B. Zhan, Y.-H. Lin, B. Zhang, X. Yuan, W. Zhang, W. Xu, and C.-W. Nan, Adv. Mater. **25**, 5086 (2013).
[8] J. Li, J. Sui, C. Barreteau, D. Berardan, N. Dragoe, W. Cai, Y. Pei, and L.-D. Zhao, J. Alloy Compd. **551**, 649 (2013).
[9] Y.-L. Pei, J. He, J.-F. Li, F. Li, Q. Liu, W. Pan, C. Barreteau, D. Berardan, N. Dragoe, and L.-D. Zhao, NPG Asia Mater. **5**, e47 (2013).
[10] G. Ren, S. Butt, C. Zeng, Y. Liu, B. Zhan, J. Lan, Y. Lin, and C. Nan, J. Electron Mater. **44**, 1627 (2015).
[11] Y. Liu, J. Ding, B. Xu, J. Lan, Y. Zheng, B. Zhan, B. Zhang, Y. Lin, and C. Nan, Appl. Phys. Lett. **106**, 233903 (2015).
[12] Y. Liu, L.-D. Zhao, Y. Liu, J. Lan, W. Xu, F. Li, B.-P. Zhang, D. Berardan, N. Dragoe, Y.-H. Lin *et al.*, J. Am. Chem. Soc. **133**, 20112 (2011).
[13] Z. Li, C. Xiao, S. Fan, Y. Deng, W. Zhang, B. Ye, and Y. Xie, J. Am. Chem. Soc. **137**, 6587 (2015).

[14] S. Baroni, S. de Gironcoli, A. Dal Corso and P. Giannozzi, http://www.pwscf.org
[15] S. K. Saha, U. V. Waghmare, H. R. Krishnamurthy, and A. K. Sood, Phys. Rev. B **76**, 201404(R) (2007).
[16] A. Aravindh *et al.*, Solid State Commun. **144**, 273 (2007).
[17] K. L. Kostov, S. Polzin, S. K. Saha, O. Brovko, V. Stepanyuk, and W. Widdra, Phys. Rev. B **87**, 235416 (2013).
[18] S. K. Saha, S. Manna, V. S. Stepanyuk, and J. Kirschner, Sci. Rep. **5**, 12847 (2015).
[19] A. Dal Corso, Comput. Mater. Sci. **95**, 337 (2014).
[20] S. K. Saha, S. Manna, M. Przybylski, V. S. Stepanyuk, and J. Kirschner, Phys. Rev. B **90**, 081404(R) (2014).
[21] S. K. Saha, V. S. Stepanyuk, and J. Kirschner, Phys. Lett. A **378**, 3642 (2014).
[22] http://www.library.cornell.edu/nr/bookcpdf/c10-7.pdf
[23] Y. Kamihara, H. Hiramatsu, M. Hirano, R. Kawamura, H. Yanagi, T. Kamiya, and H. Hosono, J. Am. Chem. Soc. **128**, 10012 (2006).
[24] A. M. Kusainova, P. S. Berdonosov, L. G. Akselrud, L. N. Kholodkovskaya, V. A. Dolgikh, and B. A. Popovkin, J. Solid State Chem. **112**, 189 (1994).
[25] P. S. Berdonosov, A. M. Kusainova, L. N. Kholodkovskaya, V. A. Dolgikh, L. G. Akselrud, and B. A. Popovkin, J. Solid State Chem. **118**, 74 (1995).
[26] K. Ueda and H. Hosono, Thin Solid Films **411**, 115 (2002).
[27] L. D. Zhao, D. Berardan, Y. L. Pei, C. Byl, L. Pinsard-Gaudart, and N. Dragoe, Appl. Phys. Lett. **97**, 092118 (2010).
[28] B. M. Ocko, O. M. Magnussen, J. X. Wang, and R. R. Adzic, in *Nanoscale Probes of the Solid/Liquid Interface*, edited by A. A. Gewirth and H. Siegenthaler, Series E, Applied Sciences (Kluwer Academic, Dordrecht, 1995), Vol. 288, p. 115.
[29] R. D. Shannon, Acta Crystallogr., Sect. A **32**, 751 (1976).
[30] A. Walsh, D. J. Payne, R. G. Egdell, and G. W. Watson, Chem. Soc. Rev. **40**, 4455 (2011).
[31] A. Savin, O. Jepsen, J. Flad, O. K. Andersen, H. Preuss, and H. G. von Schneiring, Angew. Chem. Int. Ed. Engl. **31**, 187 (1992).
[32] G. Henkelman, A. Arnaldsson, and H. Jónsson, Comput. Mater. Sci. **36**, 354 (2006).
[33] S. C. Abrahams and J. L. Bernstein, J. Chem. Phys. **61**, 1140 (1974).
[34] D. J. Singh and I. I. Mazin, Phys. Rev. B **56**, R1650 (1997).
[35] W. Voigt, *Lehrbuch der Kristallphysik* (Teubner, Leipzig, 1928).
[36] A. Reuss, Z. Angew. Math. Mech. **9**, 49 (1929).
[37] R. Hill, Proc. Phys. Soc. London, Sect. A **65**, 349 (1952).
[38] S. F. Pugh, Philos. Mag. **45**, 833 (1954).
[39] P. Ravindran, L. Fast, P. A. Korzhavyi, B. Johansson, J. Wills, and O. Eriksson, J. Appl. Phys. **84**, 4891 (1998).
[40] J. Haines, J. M. Leger, and G. Bocquillon, Annu. Rev. Mater. Res. **31**, 1 (2001).
[41] P. Debye, Ann. Phys. **344**, 789 (1912).
[42] F. Li, J. F. Li, L. D. Zhao, K. Xiang, Y. Liu, B. P. Zhang, Y. H. Lin, C. W. Nan, and H. M. Zhu, Energy Environ. Sci. **5**, 7188 (2012).
[43] D. S. Sanditov, A. A. Mashanov, and M. V. Darmaev, Tech. Phys. **54**, 1398 (2009).
[44] A. F. Ioffe, *Physics of Semiconductors* (Infosearch, London, 1958).
[45] M. Di Gennaro, S. K. Saha, and M. J. Verstraete, Phys. Rev. Lett. **111**, 025503 (2013).
[46] G. A. Slack, J. Phys. Chem. Solids **34**, 321 (1973).
[47] M. Yasukawa, K. Ueda, and H. Hosono, J. Appl. Phys. **95**, 3594 (2004).
[48] G. Dutta, S. K. Saha, and U. V. Waghmare, Solid State Commun. **150**, 2020 (2010).
[49] S. K. Saha, Phys. Rev. B **92**, 041202(R) (2015).
[50] L. I. Anatychuk and V. P. Mikhalchenko, J. Thermoelectr. **13**, 31 (2002).
[51] J. F. Nye, *Physical Properties of Crystals* (Oxford University Press, Oxford, UK, 1985).